High thermoelectric performance in low-cost SnS0.91Se0.09 crystals

October 8 2019, by Thamarasee Jeewandara

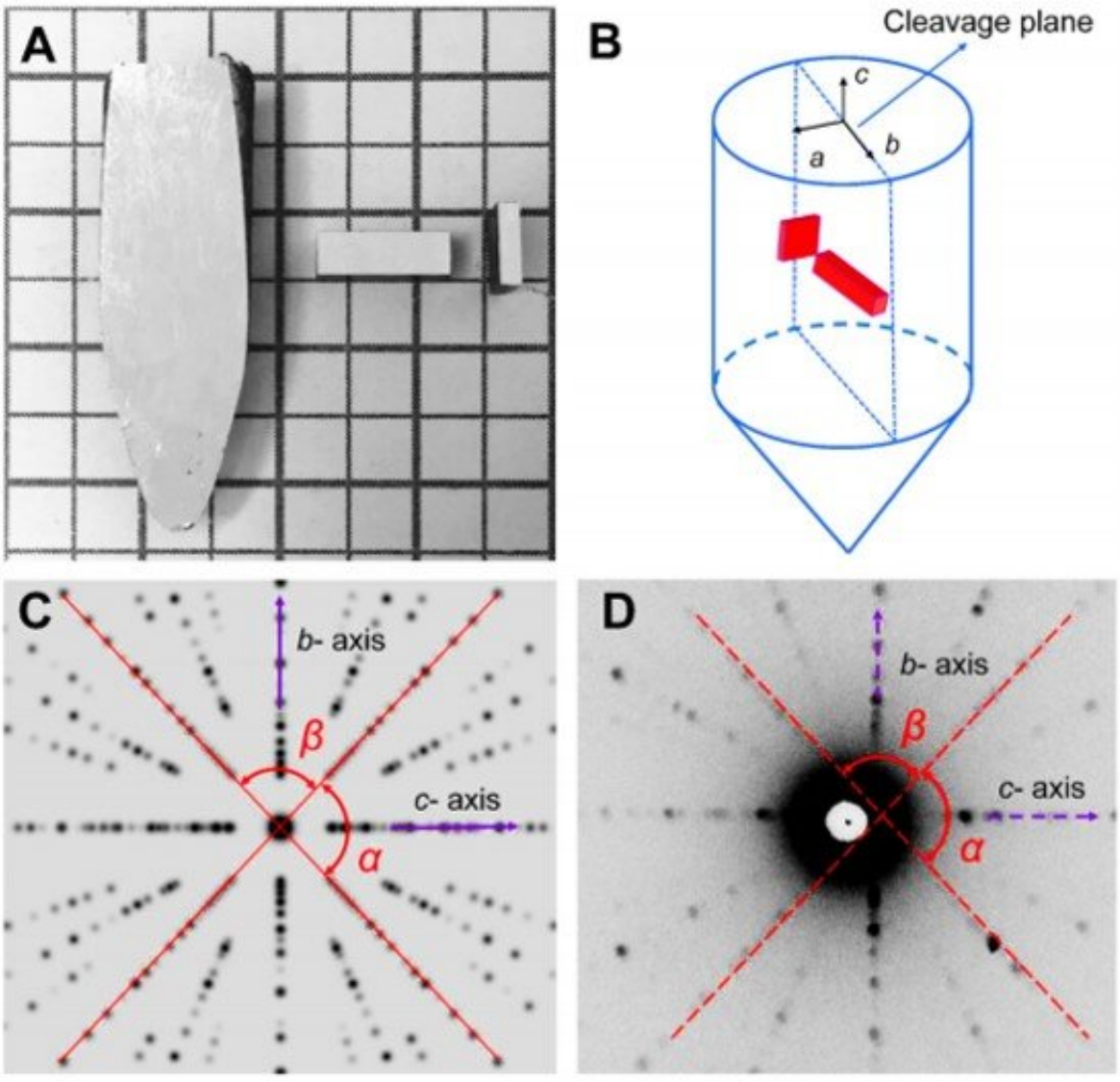

(A) A typical crystal cleaved along the (100) plane, and sample cut along b-axis. (B) A diagram shows how samples cut along b-axis for measurements. (C)

Standard Laue diffraction image of SnS crystal along [100] direction. (D) Experimentally obtained Laue diffraction pattern of SnS crystal along [100] direction. The in-plane (b-c plane) directions of SnS crystal can be determined by using the standard diffraction image as a reference. Credit: Science Advances, doi: 10.1126/science.aax5123

Thermoelectric materials technology can convert between heat and electricity within a materials construct, but many existing materials contain rare or toxic elements. In a new study on *Science*, Wenke He and colleagues reported the temperature dependent interplay between three separate electronic bands in hole-doped tin sulfide (SnS) crystals. The materials behaviour allowed synergistic optimization between effective mass (m^*) and carrier mobility (μ), which the research team boosted by introducing selenium (Se).

By alloying Se, they enhanced the power factor of the materials from approximately 30 to 53 microwatts per centimeter per square Kelvin ($\mu W cm^{-1} K^{-2}$ at 300 K) and lowered the thermal conductivity. The research team obtained a maximum figure of merit ZT (ZT_{max}) approximating 1.6 at 873 K and an average ZT (ZT_{ave}; dimensionless figure of merit) approximating 1.25 between 300 K to 837 K within $SnS_{0.91}Se_{0.09}$ crystals. The researchers introduced a strategy for bond manipulation, which offered a different route to optimize thermoelectric performance. The high-performance SnS crystals used in the work represented an important step toward developing low-cost, earth abundant and environmentally favorable thermoelectrics.

Thermoelectric technology allows the invertible conversion between thermal energy and electricity to provide an environmentally friendly route for power generation. The process can occur by harvesting waste heat or by solid-state cooling. Materials scientists and physicists have

determined the conversion efficiency of thermoelectric technology using the dimensionless figure of merit (ZT) for a given thermoelectric material. The parameters that determine the conversion efficiency of thermoelectric technology are intertwined, making the manipulation of any single parameter to improve thermoelectric performance a challenge. Researchers had already devised several strategies to improve ZTs, by optimizing power factors via band convergence, band flattening or density of states distortion.

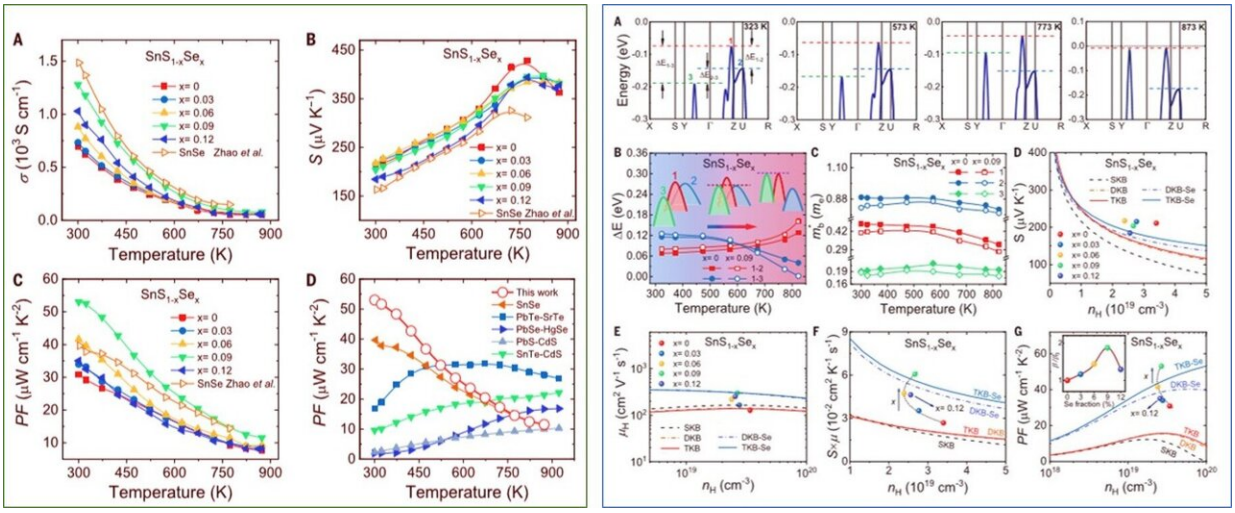

LEFT: Electrical transport properties as a function of temperature for SnS1-xSex crystals. (A) Electrical conductivity. (B) Seebeck coefficient. (C) Power factor. The electrical properties of SnSe crystals are also added for comparison (31). (D) Power factor comparisons of p-type lead and tin chalcogenides. The power factor achieved for SnS indicates a more complex band structure of SnS than of other thermoelectrics. RIGHT: Temperature-dependent electronic band structure and theoretical simulations on electrical transport properties. (A) Electronic band structure as a function of temperature. (B) Schematic of dynamic evolution of three separate valence bands with increasing temperature for SnS. (Top) As the temperature increases, VBM2 (blue) separates away from VBM1 (red), while VBM3 (green) approaches VBM1, and VBM2 crosses VBM3. (Bottom) The energy gap (DE) between VBM1 and VBM2, and between VBM1 and VBM3, as a function of temperature in SnS1-xSex. (C) The effective masses as a function

of temperature for VBM1, VBM2, and VBM3 in SnS1-xSex, indicating that effective masses decrease after Se alloying. (D) Pisarenko plots showing the Seebeck coefficients as a function of carrier concentration with different band models. (E) Carrier mobility as a function of carrier concentration with different band models. (F) The product of the Seebeck coefficient and carrier mobility as a function of carrier concentration in SnS1-xSex crystals, elucidating the advanced interplay of three separate bands. (G) The simulated power factor as a function of carrier concentration with different band models. The inset shows the ratio of quality factor (b/b0) in SnS 1-xSex crystals to that in SnS. The experimental data are consistent with the simulations with the TKB model, indicating the contribution of three bands. SKB indicates a single Kane band; DKB, a double Kane band; and TKB, a triple Kane band. Credit: Science Advances, doi: 10.1126/science.aax5123

Scientists can decouple thermoelectric parameters by embedding magnetic nanoparticles and reduce thermal conductivity with nanostructures. Materials scientists have also developed entirely new materials with intrinsically low thermal conductivity or with a large power factor, or with high-performance thermoelectrics sourced via reliable high-throughput material screening. High-performance thermoelectrics are typically widely studied across group IV-VI semiconductors. The addition of SnSe (Tin selenide) to the group is promising since thermoelectric materials do not contain these elements. Furthermore, SnSe has properties of a high ZT alongside multiple valence bands and three-dimensional (3-D) charge and 2-D phonon transport.

The SnS compound is a structural analog of SnSe and predicted to be an attractive thermoelectric candidate as well. While the lower cost and earth abundance of S (sulfur) is appealing for frugal science and large-scale commercial applications, the low carrier mobility can cause poor electrical transport properties to impede high thermoelectric

performance. In the present work, He et al. therefore explored the thermoelectric potentials of SnS crystals by manipulating their band structure, since the research team had also previously shown the ability to boost the carrier mobility of SnS crystals. Since S was quite reactive with contact materials, it was important to develop a diffusion barrier in the future.

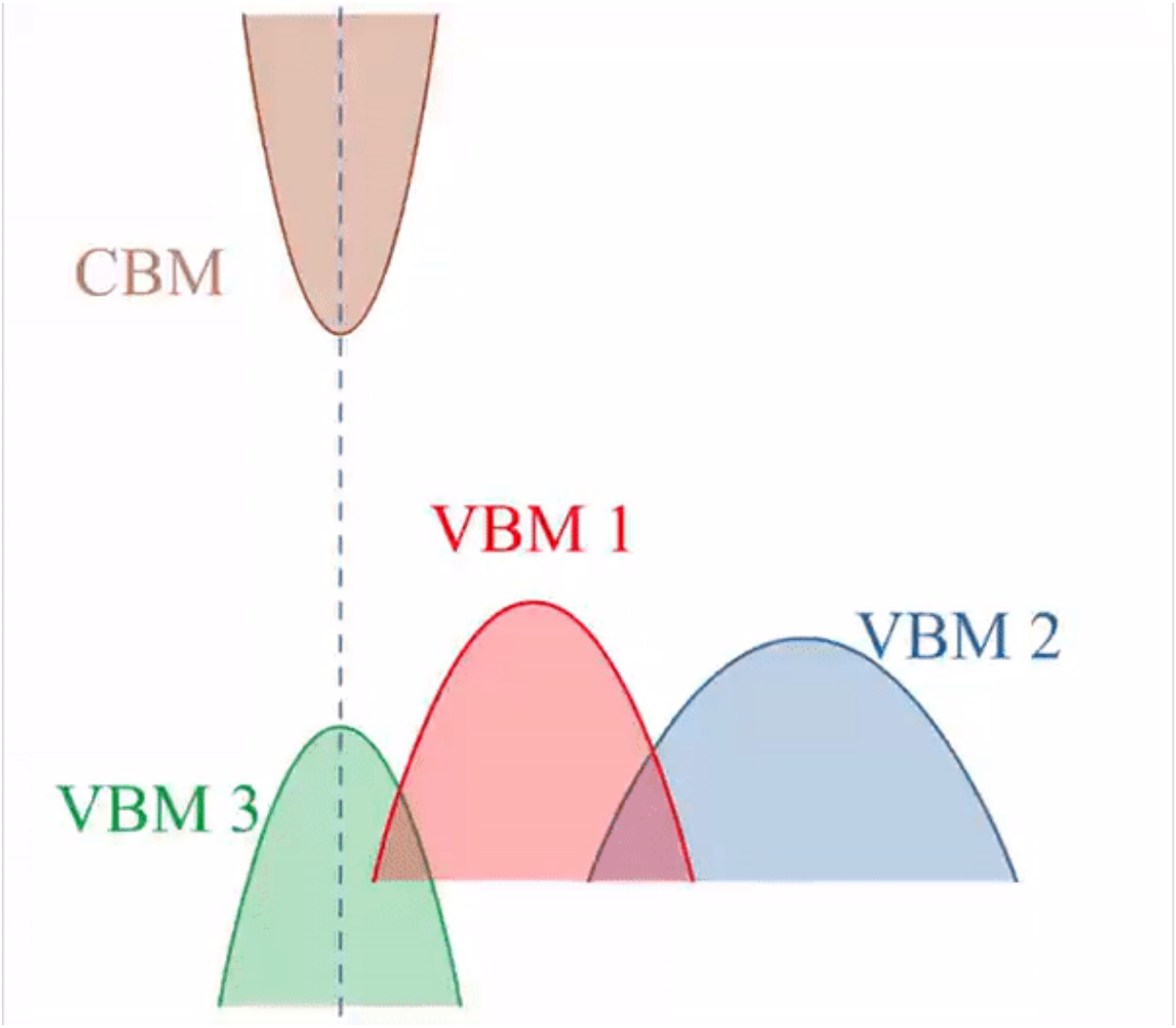

Schematic moving for the interplay of three separate valence bands in SnS. Credit: Science Advances, doi: 10.1126/science.aax5123

In the present work, the research team synthesized $SnS_{1-x}Se_x$ crystals using a temperature gradient method to investigate the role of Se in the compound. The team obtained temperature-dependent electronic band structures using density function theory calculations (DFT) based on atomic positions, which they derived using high-temperature synchrotron radiation X-ray diffraction (SR-XRD) data. Using the DFT calculations and angle-resolved photoemission spectroscopy measurements (ARPES), the team confirmed three separate electronic band interactions. They promoted the outstanding behavior interplay of the electronic bands by substituting S with Se to successfully optimize the effective mass (m^*) and effective mobility (μ) within the material. They enhanced the power factor (PF) from 30 to 53 $\mu Wcm^{-1}K^{-2}$ at 300 K. The team confirmed Se substitution using aberration-corrected scanning transmission electron microscopy (STEM) and X-ray absorption fine structure spectroscopy (XAFS). Using inelastic neutron scattering (INS), He et al. showed that typical phonons (acoustic waves) were softened by Se substitution and further coupled with acoustic branches for lower thermal conductivity.

The results further implied that the electrical conductivity improved due to enhanced carrier mobility after alloying 9 percent Se. The research team observed a combined increase in electrical conductivity and a large Seebeck coefficient (thermoelectric sensitivity) to provide a PF (power factor) approximating 53 $\mu Wcm^{-1}K^{-2}$ at 300 K for the $SnS_{0.91}Se_{0.09}$ crystals. The values were higher than those of other thermoelectric materials in the group IV to VI compounds. The research team schematically illustrated the dynamic evolution of the three valence bands and the energy offset between them as a function of temperature. Then by introducing Se, He et al. promoted the interplay of the three valence bands responsible to optimize the effective mass and mobility (m^* and μ); where lowering m^* resulted in improving μ.

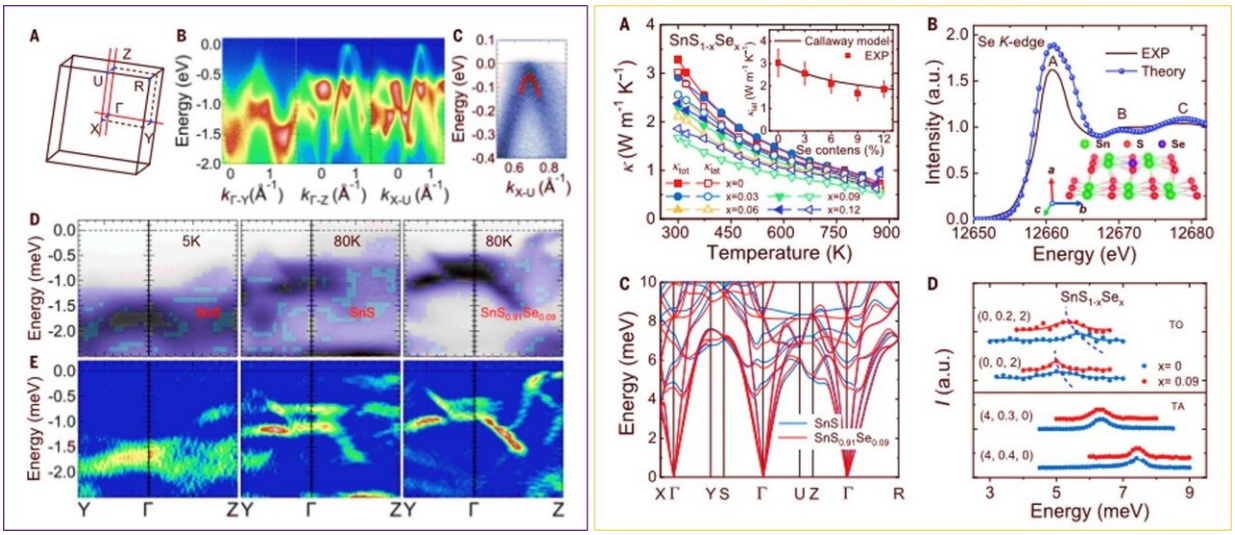

LEFT: Brillouin zone and band structures observed by ARPES. (A) Brillouin zone of SnS, and sketch of the three cuts in the Brillouin zone. (B) ARPES band structures of SnS along the G-Y, G-Z, and X-U directions. The VBM3 (G-Y) is located at E3 = −0.30 eV, VBM1 (G-Z) is located at the Fermi level (E1 = 0 eV), and VBM2 (X-U) is located at E2 = −0.05 eV. Three cuts illustrate the band dispersion of the three VBMs in SnS. (C) ARPES band structure along the X-U direction. Parabolic fit of the energy distribution curve gives VBM2 at k = 0.69 Å −1, E2 = −0.05 eV. (D) Electronic band structures for SnS1-xSex (x = 0, 0.09) along the Y-G-Z plane at 5 and 80 K, respectively. The energy gaps (DE) between VBM1 and VBM2 are 0.50 eV (5 K, SnS), 0.30 eV (80 K, SnS), and 0.15 eV (80 K, SnS0.91Se0.09), respectively. (E) Second derivative maps (with respect to energy) along the Y - G- Z plane for SnS1-xSex (x = 0, 0.09). RIGHT: Thermal conductivity as a function of temperature and phonon band structure. (A) Total and lattice thermal conductivity for SnS1-xSex crystals. Inset shows the room temperature lattice thermal conductivities fitted with the Callaway model. (B) Comparison of the experimental and theoretical Se K-edge XANES spectra. Inset: A sketch of the atomic structure indicating Se substituting for S in SnS. (C) Phonon band structure of SnS1-xSex (x = 0, 0.09). (D) Typical constant-Q scans of the TO mode at Q = (0, 0, 2) and (0, 0.2, 2), and TA mode at Q = (4, 0.3, 0) and (4, 0.4, 0), which indicates that the phonon energy of the TO mode decreases after Se alloying, whereas the TA mode changes only slightly. Credit: Science Advances, doi: 10.1126/science.aax5123

He et al. also used ARPES (angle-resolved photoemission spectroscopy measurements) to observe the electric band structure of SnS crystals. They plotted three valence bands along different directions and their relative energy levels in the 3-D Brillouin zone (a theoretical zone). The scientists then conducted X-ray absorption fine structure spectroscopy (XAFS) on $SnS_{1-x}Se_x$ crystals to understand the Se substitution. Their work showed that for $SnS_{0.91}Se_{0.09}$ crystals, the X-ray absorption near-edge structure (XANES) spectrum contained three main features. The research team reproduced all three major experimental features using a simulated spectrum and a Se substitution model. They observed the successful introduction of Se into the SnS lattice for all $SnS_{1-x}Se_x$ crystals.

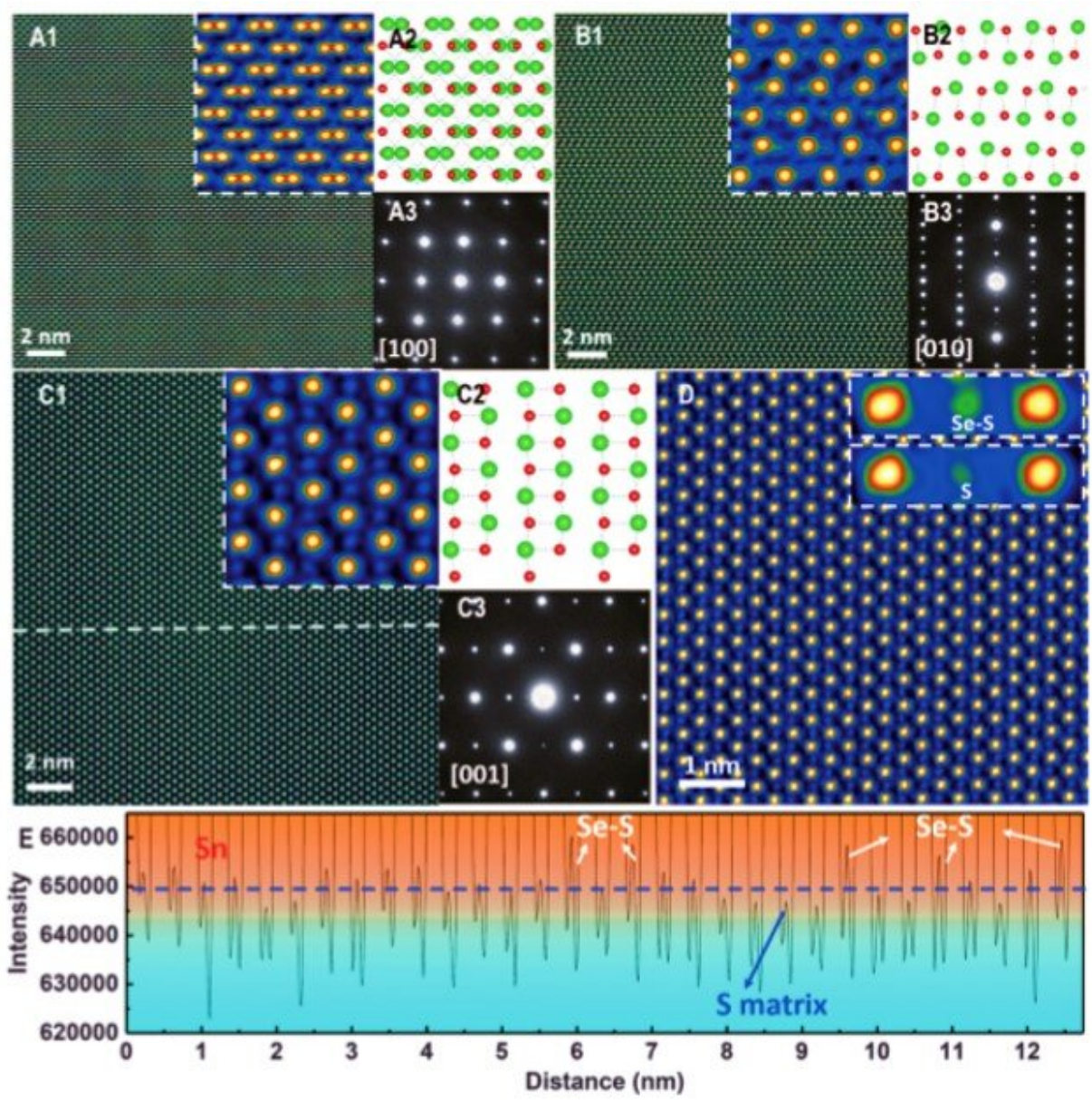

: Atomic-scale structures of high performance SnS0.91Se0.09 crystal. (A1, B1, C1) Atomically resolved STEM HAADF images along the [100], [010], and [001] zone axes, respectively, with enlarged images shown in the insets. (A2, B2, C2) The respective structural models. (A3, B3, C3) The respective electron diffraction patterns. (D) Atomically resolved STEM HAADF image along the [001] zone axis, with enlarged images showing the intensity difference between Se-substituted S and the SnS matrix. (E) Intensity profile from the dashed line of (C1) showing the higher intensity of Se-substituted S, compared with the SnS matrix. Credit: Science Advances, doi: 10.1126/science.aax5123

The team used STEM high-angle annular dark-field (HAADF) to produce a contrast image and view atomic-scale Se substitutions on S sites within $SnS_{0.91}Se_{0.09}$ crystals. They obtained structural modes and electron diffraction patterns for SnS and SnSe in dumbbell-like atomic arrangements. The abnormal brightness on the S sites indicated Se substitutions. They combined exceptionally high power factor (PF) and low thermal conductivity to generate a maximum ZT (ZT_{max}), for the $SnS_{0.91}Se_{0.09}$ crystals. He et al. showed good thermoelectric stability for the high-performance crystals, where the crystals showed excellent stability after neutron irradiation for 432 hours. Such irradiation resistance is important for radioisotope thermoelectric generators for deep-space exploration.

Compared with other group IV-VI thermoelectric materials, SnS materials were far superior relative to toxicity and elemental abundance. The researchers expect to further optimize contact materials for SnS during elemental substitution to obtain higher experimental efficiency with low cost and high-performance in the future. In this way, Wenke He and colleagues used $SnS_{0.91}Se_{0.09}$ crystals to extensively demonstrate the great potential for competitive, large-scale applications in thermoelectrics materials technology.

More information: Wenke He et al. High thermoelectric performance in low-cost SnS0.91Se0.09 crystals, *Science* (2019). DOI: 10.1126/science.aax5123

Wenyu Zhao et al. Magnetoelectric interaction and transport behaviours in magnetic nanocomposite thermoelectric materials, *Nature Nanotechnology* (2016). DOI: 10.1038/nnano.2016.182

Li-Dong Zhao et al. Ultralow thermal conductivity and high

thermoelectric figure of merit in SnSe crystals, *Nature* (2014). DOI: 10.1038/nature13184